

Empirical photometric calibration of the Gaia Red Clump: colours, effective temperature and absolute magnitude [★]

L. Ruiz-Dern, C. Babusiaux, F. Arenou, C. Turon, R. Lallement

GEPI, Observatoire de Paris, PSL Research University, CNRS UMR 8111 - 5 Place Jules Janssen, 92190 Meudon, France

Received 17 July 2017; Accepted 16 October 2017

ABSTRACT

Context. Gaia Data Release 1 allows to recalibrate standard candles such as the Red Clump stars. To use those, they first need to be accurately characterised. In particular, colours are needed to derive the interstellar extinction. As no filter is available for the first Gaia data release and to avoid the atmosphere model mismatch, an empirical calibration is unavoidable.

Aims. The purpose of this work is to provide the first complete and robust photometric empirical calibration of the Gaia Red Clump stars of the solar neighbourhood, through colour-colour, effective temperature-colour and absolute magnitude-colour relations, from the Gaia, Johnson, 2MASS, Hipparcos, Tycho-2, APASS-SLOAN and WISE photometric systems, and the APOGEE DR13 spectroscopic temperatures.

Methods. We used a 3D extinction map to select low reddening red giants. To calibrate the colour-colour and the effective temperature-colour relations, we developed a MCMC method which accounts for all variable uncertainties and selects the best model for each photometric relation. We estimate the Red Clump absolute magnitude through the mode of a kernel-based distribution function.

Results. We provide 20 colour vs $G - K_s$ relations and the first T_{eff} vs $G - K_s$ calibration. We obtained the Red Clump absolute magnitudes for 15 photometric bands with, in particular, $M_{K_s} = (-1.606 \pm 0.009)$ and $M_G = (0.495 \pm 0.009) + (1.121 \pm 0.128) (G - K_s - 2.1)$. We present an unreddened Gaia-TGAS HR diagram and use the calibrations to compare its Red Clump and its Red Giant Branch Bump with the Padova isochrones.

Key words. stars: fundamental parameters - stars: abundances - stars: atmospheres - ISM: dust, extinction

1. Introduction

Measuring distances with high accuracy is as difficult as fundamental in astronomy. The most direct method for estimating astronomical distances is the trigonometric parallax. However, relative precisions of parallaxes decrease with distance. In order to go further we need to use standard candles such as Red Clump (hereafter RC) stars.

RC stars are low mass core *He*-burning (CHeB) stars and cooler than the instability strip. They appear as an overdensity in the Colour-Magnitude Diagram (CMD) of populations with ages older than $\sim 0.5 - 1$ Gyr, covering the range of spectral types G8III - K2III with $4500\text{K} \lesssim T_{\text{eff}} \lesssim 5300\text{K}$. Indeed, the RC represents the young and metal-rich counterpart of the Horizontal Branch (see Girardi 2016, for a review).

The Red Clump is used as a standard candle for estimating astronomical distances due to its relatively small dependency of the luminosity on the stellar composition, colour and age in the solar neighbourhood (Paczynski & Stanek 1998; Stanek & Garnavich 1998; Udalski 2000; Alves 2000; Groenewegen 2008; Valentini & Munari 2010). As stated by Paczynski & Stanek (1998), any method to obtain distances to large-scale structures suffers mainly from four problems: the accuracy of the absolute magnitude determination of the stars used, the interstellar extinction, the distribution of the inner properties of these stars (mass, age, chemical composition), and how large the sample is. Whether the use of the RC may be considered particularly different than other standard candles such as RR Lyrae or Cepheids, is

precisely due to their large number. The larger the sample used, the lower the statistical error in distance calculations. To efficiently use the Red Clump as a standard candle, a good characterisation of the calibrating samples, here the solar neighbourhood, is needed, to which stellar population corrections can then be applied (see e.g. Girardi et al. 1998).

The First Gaia Data Release (GDR1) was delivered to the scientific community in September 2016 (Gaia Collaboration et al. 2016a,b). Although we will have new and more accurate astrometric and photometric measurements for thousands of RC stars in future releases, this first catalogue includes the Tycho-Gaia Astrometric Solution (TGAS) subsample (Lindgren et al. 2016) with already a significant set of accurate solar neighbourhood RC parallaxes (with systematic error at the level of 0.3 mas, i.e. 3 times better than in the Hipparcos catalogue, for 20 times more stars).

By comparing the observations with isochrones we can directly constrain stellar parameters such as ages and metallicities. However, we found that at the level of red giant stars, atmosphere models and observations do not fit: there is a *gap* between them no matter the photometric bands nor the atmosphere models used. As an example, we show this issue in Fig. 1 for the $B - V$ vs $V - I$ and $J - K_s$ vs $V - K_s$ colour-colour diagrams of some RC stars, and for both *Padova* (Parsec 2.7) and *Dartmouth* isochrones, who use *ATLAS* and *Phoenix* atmosphere models, respectively. A more exhaustive work on the important effects on the choice of atmosphere models and other parameters may be found in Aringer et al. (2016). We have checked that a unique shift is not enough to correct this *gap* because the slope is also different. We have also checked the influence of filter modelling.

Send offprint requests to: laura.ruiz-dern@obspm.fr

[★] Table A.1 is only available in electronic form at the CDS

Nevertheless, it seems that it is most probably an issue of atmosphere models.

Therefore there are two aspects that led us to develop the purely empirical calibrations that we present in this work: 1) the need of a photometric calibration totally independent of models, and 2) the fact that there is no on-board Gaia calibrated filter profile (instrumental response) available for the GDR1, thus a colour-colour calibration was automatically needed. Jordi et al. (2010) already predicted some colour relationships based on theoretical spectra and the nominal Gaia passbands (calibrated before launch), but the effective filters actually slightly differ (van Leeuwen et al. 2017). Therefore, there is an special interest in using colour-colour empirical calibrations instead.

In this work we present the first metallicity-dependent empirical colour-colour (hereafter *CC*), effective temperature (T_{eff} -colour and colour- T_{eff} , hereafter $T_{\text{eff}}C$ and CT_{eff} respectively) and absolute magnitude (M_G and M_K) calibrations for solar neighbourhood RC stars using the Gaia *G* magnitude.

The paper is organized as follows. In Sect. 2 we describe the sample selection, the adopted constraints and how the interstellar extinction has been handled. The method developed to calibrate all the *CC* and T_{eff} relations is explained in Sect. 3. The calibrations obtained are presented in Sect. 4. In Sect. 5 we detail the RC absolute magnitude calibration. And finally in Sect. 6 we present the un-reddened TGAS HR diagram and compare its RC to the Padova isochrones.

2. Sample selection

Different samples were constructed using TGAS data for the colour-colour and the effective temperature calibrations. To ensure their quality we considered the following constraints.

2.1. Interstellar extinction

One of the main issues with *CC*, $T_{\text{eff}}C$ and CT_{eff} calibrations for giants is the extinction handling. To select low extinction stars, we use here the most up-to-date 3D local extinction map of Lallement et al. (2014), Capitanio et al. (2017), together with the 2D Schlegel et al. (1998) map for stars for which the distance go beyond the 3D map borders. We scaled the Schlegel et al. (1998) map values by 0.884 according to Schlafly & Finkbeiner (2011) and in agreement with the Capitanio et al. (2017) $E(B - V)$ scale. We fixed a maximum threshold of 0.01 in $E(B - V)$ (i.e. 0.03 in A_0) for a maximum distance corresponding to a parallax $\varpi - \sigma_\varpi$. Such a selection of low extinction stars should lead to more robust results than a dereddening that would be dependent not only on an extinction map but also on an extinction law, and could lead to either over or under correction of the extinction.

2.2. Red Giants selection

To select solar neighbourhood red giant stars we considered the following two criteria:

$$G - K_s > 1.6 \quad (1)$$

$$m_G + 5 + 5 \log_{10} \left(\frac{\varpi + 2.32 \sigma_\varpi}{1000} \right) < 4.0 \quad (2)$$

The factor 2.32 on the parallax error corresponds to the 99th percentile of the parallax probability density function. Fig. 2

shows the selected region on the HR diagram. The data used to construct this HR diagram is described in Appendix A, Table A.1. See Sect. 6 for more details on the RC region of this diagram.

We extended the parallax criteria to cover the full red giant branch so that our calibrations have a larger interval of applicability than just the Red Clump. We checked that this large magnitude interval did not have any significant impact on the calibration. The fit is on the opposite very sensitive to red dwarf stars contaminants. Indeed the slope of giants and dwarfs in colour-colour distributions changes gradually as the stars are cooler (e.g. Bessell & Brett 1988). A selection based on spectroscopic surface gravity ($2.5 < \log g < 3.5$) was tested and discarded due to the non-negligible percentage of giants/dwarfs misidentification in some surveys (e.g. we found $\sim 2\%$ misidentified RAVE stars when selecting those matching Appendix A criteria and supposed to be inside the non-shaded region of Fig. 2). The chosen parallax criteria allows us to guarantee there is no dwarfs' contamination in our sample.

2.3. Photometric data

Our calibrations aim to cover all major visual and infrared bands. To achieve this we selected only those DR1 stars which have photometric information (with uncertainties) from the following catalogues:

2.3.1. GDR1

G band with uncertainties lower than 0.01 mag. An error of 10 mmag was quadratically added to mitigate the impact of bright stars residual systematics, see Arenou et al. (2017); Evans et al. (2017).

2.3.2. Hipparcos

B, *V* and *H_p* bands with uncertainties lower than 0.03 mag. We did not include the *I* band because of the low number (~ 12) of remaining stars when selecting those with $V - I$ direct measurements in the Cousin's system (field $H42 = A$), with measurements in the Johnson's system then converted to Cousin's (field $H42 = C$), and with measurements in the Kron-Eggen's system then converted to Cousin's (field $H42 = E$). For more details see Perryman et al. (1997), Vol. 1, Sect. 1.3, Appendix 5.

2.3.3. Tycho-2

B_T and V_T bands (Høg et al. 2000) with uncertainties lower than 0.03 mag.

2.3.4. 2MASS

J, *H* and *K_s* bands (Cutri et al. 2003) from the crossmatched 2MASS-GDR1 catalogue (Marrese et al. 2017, submitted) with high photometric quality (i.e. flag q2M = A) and from Laney et al. (2012). Only stars with uncertainties lower than 0.03 mag.

2.3.5. APASS DR9

g, *r* and *i* bands (Henden et al. 2016) crossmatched with Gaia at $2''$ precision, and only stars with standard deviations obtained from more than one observation ($u_e = 0$ flag in the APASS catalogue) and uncertainties lower than 0.03 mag. Duplicates were

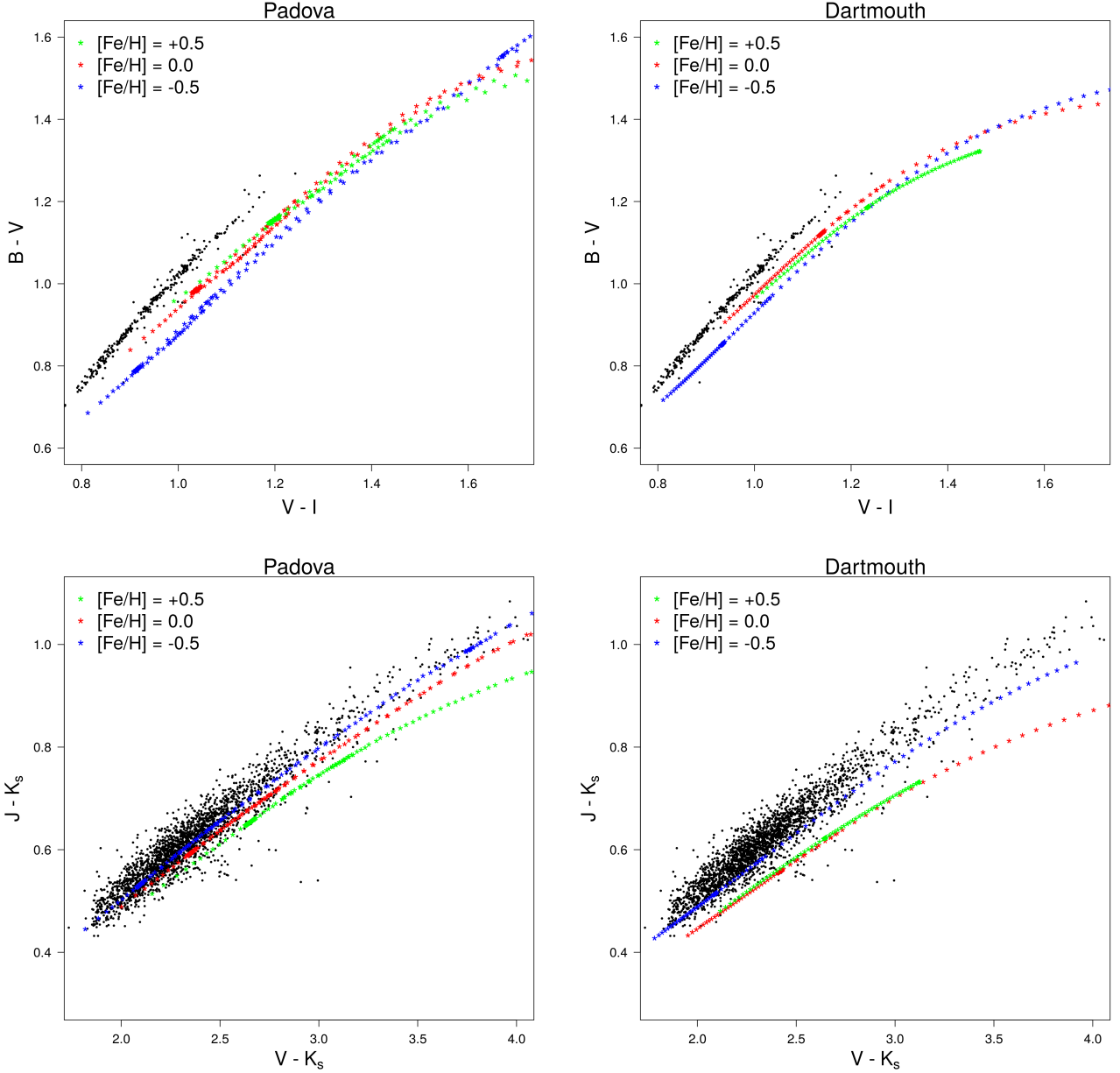


Fig. 1. $B-V$ vs $V-I$ and $J-K_s$ vs $V-K_s$ colour-colour diagrams of RC stars (sample described in Section 2). The median metallicity of the sample is about -0.2. *Padova* Parsec 2.7 (left) and *Dartmouth* (right) isochrones with a median age of 2Gyr are overplotted for three different metallicities: (green) $[Fe/H] = +0.5$, (red) $[Fe/H] = 0.0$, (blue) $[Fe/H] = -0.5$. Only the Red Giant Branch and the Early Asymptotic Giant Branch are shown

removed by keeping the source with the largest number of photometric bands provided in APASS.

2.3.6. WISE

W1, W2, W3 and W4 bands (Wright et al. 2010) from the cross-matched WISE-GDR1 catalogue (Marrese et al. 2017, submitted) with uncertainties lower than 0.05 mag, high photometric quality (i.e. flag qph = A), low probability of being true variables (i.e. flag var < 7), a source shape consistent with a point-source (i.e. flag ex = 0) and showing no contamination from artifacts (i.e. flag ccf = 0). According to Cotten & Song (2016), for W2 we also removed stars brighter than 7 mag, because they are saturated.

2.4. Binarity and Multiplicity

We removed all stars flagged as binaries and belonging to multiple systems. To do so we took into account the specific flags in the *Hipparcos* catalogue as well as the last updated information from:

- *9th Catalogue of Spectroscopic Binary Orbits* (SB9, Pourbaix et al. 2004, 2009)
- *The Tycho Double Star Catalogue* (TDSC, Fabricius et al. 2002)
- Simbad database (stars with flag "**")
- We also considered only stars for which the proper motions from *Hipparcos* are consistent with those of Tycho-2 (rejection p-value: 0.001). According to a specific test carried out in the framework of the Gaia data validation team (Arenou

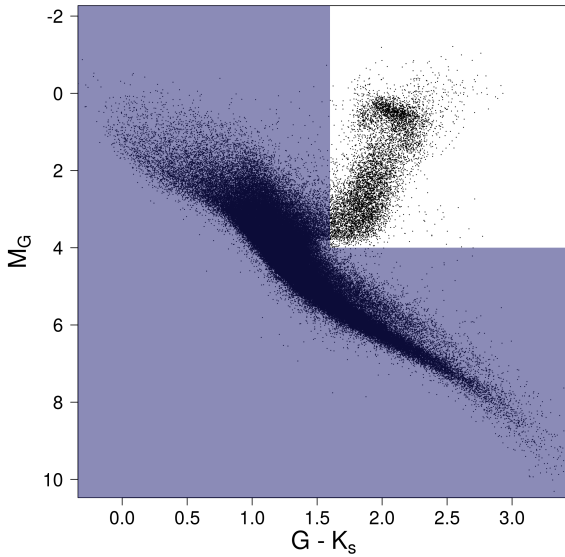


Fig. 2. TGAS HR diagram with parallax precision $\leq 10\%$, $\sigma_G < 0.01$, $E_{B-V} < 0.015$ and 2MASS JK -bands high photometric quality (data available in Table A.1, Appendix A). The non-shaded region corresponds to the Red Giants selection, with $G - K_s > 1.6$ and $M_G < 4.0$

et al. 2017) most of the stars for which the proper motions are not consistent between both catalogues, are expected to be long period binaries not detected in Hipparcos, and for which the longer time baseline of Tycho-2 could have provided a more accurate value.

2.5. Metallicity

We selected stars with metallicity information from different sources, since there were not enough stars when using just one reference. We expect the differences between all the measurements to increase the dispersion of the residuals and to decrease the dependence of the calibrations with metallicity. Noting in brackets the percentage of stars found and used in this work¹, our established priority order is: Morel et al. (2014) [0%], Thygesen et al. (2012) [0%], Bruntt et al. (2012) [0.04%], Maldonado & Villaver (2016) [0.6%], Alves et al. (2015) [1.4%], Jofré et al. (2015) [0.4%], Bensby et al. (2014) [0.4%], da Silva et al. (2015) [0.04%], Mortier et al. (2013) [0.04%], Adibekyan et al. (2012) [0.3%], APOGEE DR13 (SDSS Collaboration et al. 2016) [9.9%], GALAH (Martell et al. 2017) [0.4%], Ramírez et al. (2014a) [0%], Ramírez et al. (2014b) [0%], Ramírez et al. (2013) [0.04%], Zięliński et al. (2012) [0.2%], Puzeras et al. (2010) [0.04%], Takeda et al. (2008) [0.08%], Valentini & Munari (2010) [0.6%], Saguner et al. (2011) [0%], RAVE DR5 (Kunder et al. 2017) [67.6%], LAMOST DR2 (Luo et al. 2016) [13.5%], AMBRE DR1 (De Pascale et al. 2014) [1.0%], Luck (2015) [0.7%], PASTEL (Soubiran et al. 2016) [2.8%].

The final sample contained 2334 stars when considering the extinction, red giants selection, multiplicity, metallicity and the photometric constraints on the G and K_s bands. Subsamples were then generated for each colour-colour relation depending on the other photometric bands used (see later in Table 4 the final sizes for every fit).

¹ Note that some references used in our compilation could lead to no star in the final sample, i.e. 0%, due to the various quality cuts

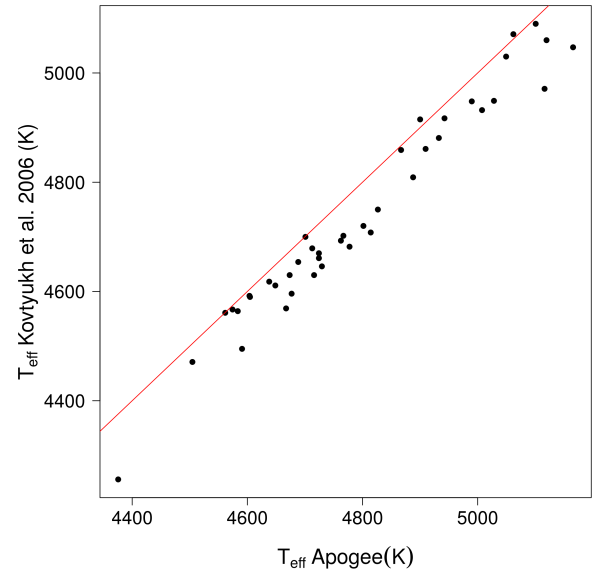


Fig. 3. Comparison of the spectroscopic effective temperatures of the 41 stars in common between APOGEE and Kovtyukh et al. (2006)

2.6. Effective Temperature

For the T_{eff} calibrations the largest homogeneous sample filling all the above criteria is the 13th release (DR13) of the APOGEE survey (Holtzman et al. 2015; García Pérez et al. 2016; SDSS Collaboration et al. 2016). To increase the sample size, we also include stars not in TGAS with APOGEE $\log g < 3.2$, using therefore only the Schlegel et al. (1998) map to apply our low extinction criteria. The weighted mean of the parameters is computed for the duplicated sources. The cross-match with Gaia is done through the 2MASS cross-match (Marrese et al. 2017, submitted) with an angular distance $< 1''$. The final sample contained 530 stars.

The SDSS Collaboration discuss a systematic offset² of their spectroscopic effective temperatures from photometrically-derived temperatures for metal-poor stars (by as much as 200–300 K for stars at $[\text{Fe}/\text{H}] \sim -2$). Consequently they provided a correction as a function of metallicity. We decided not to apply their suggested correction as it is based on comparison with photometric temperatures. We compared the APOGEE temperatures to the PASTEL ones and see metallicity correlations only for the most metal-poor stars ($[\text{Fe}/\text{H}] < -1.5$). We tested that our calibrations did not change significantly when we removed the most metal-poor stars from our sample.

For metal-rich stars, we compared 41 giant stars (within $-0.4 < [\text{Fe}/\text{H}] < 0.2$) from Kovtyukh et al. (2006) in common with APOGEE. They got a very good internal precision of 5–20 K (zero-point difference expected to be smaller than 50 K). As shown in Fig. 3 we find a difference of about 50 K with respect to APOGEE, with no correlation with $[\text{Fe}/\text{H}]$, and a dispersion in agreement with the precisions provided in both catalogues.

3. Calibration method

To derive accurate photometric relations, we implemented a Monte Carlo Markov Chain (MCMC) method which allows us

² <http://www.sdss.org/dr13/irspec/parameters/\#QualityoftheASPCAPStellarParameters>

to account and deal with the uncertainties of both the predictor and response variables in a robust way.

We provide all the calibrations with respect to the $G - K_s$ colour. Those photometric bands will be widely used thanks to the all-sky and high uniformity properties of the Gaia and 2MASS catalogues. Thus, in this work we provide the following calibrations:

$$\begin{aligned} \text{Colour} &= f(G - K_s, [\text{Fe}/\text{H}]) \\ \hat{T} &= f(G - K_s, [\text{Fe}/\text{H}]) \\ G - K_s &= f(\hat{T}, [\text{Fe}/\text{H}]) \end{aligned} \quad (3)$$

where *Colour* includes all possible combinations of the photometric bands considered in this work (Section 2.3), and $\hat{T} = T_{\text{eff}}/5040$ is the normalised effective temperature.

3.1. Polynomial models

The general fitting formula adopted is:

$$Y = a_0 + a_1 X + a_2 X^2 + a_3 [\text{Fe}/\text{H}] + a_4 [\text{Fe}/\text{H}]^2 + a_5 X [\text{Fe}/\text{H}] \quad (4)$$

a second order polynomial³ where, following Eq. 3, X is either the $G - K_s$ or the normalized effective temperature \hat{T} , Y is (for CC) a given colour to be calibrated or (for T_{eff} relations) either $G - K_s$ or \hat{T} , and a_i are the coefficients to be estimated. In order to provide the most accurate fit for each relation, the process (see Sect. 3.3) penalises by the complex terms so that, in the end, seven different models may be tested for every relation (Model 7 being the more complex one):

$$\begin{aligned} \text{Model 1 : } Y &= a_0 + a_1 X \\ \text{Model 2 : } Y &= a_0 + a_1 X + a_2 X^2 \\ \text{Model 3 : } Y &= a_0 + a_1 X + a_3 [\text{Fe}/\text{H}] \\ \text{Model 4 : } Y &= a_0 + a_1 X + a_2 X^2 + a_3 [\text{Fe}/\text{H}] \\ \text{Model 5 : } Y &= a_0 + a_1 X + a_3 [\text{Fe}/\text{H}] + a_4 [\text{Fe}/\text{H}]^2 \\ \text{Model 6 : } Y &= a_0 + a_1 X + a_2 X^2 + a_3 [\text{Fe}/\text{H}] + a_4 [\text{Fe}/\text{H}]^2 \\ \text{Model 7 : } Y &= a_0 + a_1 X + a_2 X^2 + a_3 [\text{Fe}/\text{H}] + a_4 [\text{Fe}/\text{H}]^2 + a_5 X [\text{Fe}/\text{H}] \end{aligned}$$

Input uncertainties from all variables are taken into account in the model.

3.2. MCMC

A Monte Carlo Markov Chain was run for every model tested, with 10 chains and 10000 iterations for each. We used the *runjags*⁴ library from the R programme language. An uninformative prior was set through a normal distribution with zero mean and standard deviation 10. Further, we also set an initial value for every coefficient. That is, we used the output coefficients obtained for each model through a multiple linear regression (simpler method which does not take uncertainties into account, but allows to obtain approximated values). The MCMC fit is run on the standardized variables to improve the efficiency of MCMC sampling (reducing the autocorrelation in the chains). Chain convergence is checked with the Gelman and Rubin's convergence diagnostic.

³ Upper degrees were tested, but discarded by an Analysis of Variance test (ANOVA), meaning that simpler models were good enough to describe the data

⁴ <https://cran.r-project.org/web/packages/runjags/runjags.pdf>

3.3. Best model selection: DIC

The model selection was done through a process of penalisation by the complex terms. To do so we took advantage of the Deviance Information Criterion (DIC) (Plummer 2008), and we tested the models by pairs: a given complex model is compared to the next simpler model (e.g. we remove the highest-order interactions, starting with the cross-term $X * [\text{Fe}/\text{H}]$).

The method continuously determined the next pair of models to be compared, run the MCMC for each and checked their DIC. When the DIC difference was significantly negative at 1σ (i.e. $\Delta \text{DIC} + \sigma_{\Delta \text{DIC}} < 0$) the complex model was kept, else the next pair was tested.

3.4. Outliers

Once the best model determined, the method checked whether there were calibrated stars out of 3σ from the model. If so, the furthest one was removed and the complete process was run again. Outliers were eliminated one by one to ensure that the further one was not causing a deviation in the model that led to consider other stars as "false outliers".

4. Calibration results

4.1. Colour-Colour relations

Table 1 gives the coefficients for each of the 19 colour vs $G - K_s$ fit, together with the $G - K_s$ and metallicity ranges of applicability (defined by the maximum and minimum values of each individual sample), as well as the number (N) of stars used after the 3σ clipping, the percentage of outliers removed and the final root mean square deviation (RMS). Fig. 4 shows the colour vs $G - K_s$ relations obtained for four of the twenty colour indices with the residuals of the fit as a function of the colour itself and of the metallicity. The scatter obtained in the residuals is very small ($\sim \pm 0.03$ globally).

4.2. Effective Temperature calibration

Table 2 provides the coefficients of the fit for the \hat{T} vs $G - K_s$ and the $G - K_s$ vs \hat{T} calibrations. The colour, T_{eff} and metallicity ranges of applicability are specified, as well as the number (N) of stars used after the 3σ clipping, the percentage of outliers removed and the final root mean square deviation.

Figure 5 shows the \hat{T} vs $G - K_s$ relation obtained with the residuals as a function of $G - K_s$ colour index and the metallicity. Since previous works in the literature use $\theta = 5040/T_{\text{eff}}$ instead of the \hat{T} considered here (e.g. Ramírez & Meléndez (2005), González Hernández & Bonifacio (2009) or Huang et al. (2015)), we also computed the calibration by using θ . We found both calibrations look similar except for the cool stars, for which we just have a few points. We may see how in this region the \hat{T} relations at different metallicities cross each other in an unrealistic way. This does not happen for the θ fit. However, after having statistically compared both the \hat{T} and θ calibrations, we chose to provide only the coefficients for \hat{T} vs $G - K_s$. Indeed, DIC is significantly lower for the \hat{T} fit. The dispersion obtained on the T_{eff} residuals is about 59K, consistent with the uncertainties of the APOGEE data used (~ 69 K).

Table 1. Coefficients and range of applicability of colour vs $G - K_s$ relations: $Y = a_0 + a_1 (G - K_s) + a_2 (G - K_s)^2 + a_3 [\text{Fe}/\text{H}] + a_4 [\text{Fe}/\text{H}]^2 + a_5 (G - K_s) [\text{Fe}/\text{H}]$

Colour	$G - K_s$ range	[Fe/H] range	a_0	a_1	a_2	a_3	a_4	a_5	RMS	%outliers	N
B - G	[1.6, 2.4]	[-1.4, 0.4]	0.583 ± 0.180	-0.046 ± 0.187	0.215 ± 0.049	0.144 ± 0.006	-	-	0.02	17.9	230
B - V	[1.6, 2.4]	[-1.4, 0.4]	-0.094 ± 0.017	0.552 ± 0.009	-	0.129 ± 0.005	-	-	0.02	10.4	251
B - J	[1.6, 2.4]	[-1.5, 0.4]	-0.117 ± 0.041	1.432 ± 0.021	-	0.153 ± 0.011	-	-	0.03	12.9	176
B - K_s	[1.6, 2.4]	[-1.5, 0.4]	-0.161 ± 0.038	1.757 ± 0.020	-	0.141 ± 0.011	-	-	0.02	9.3	254
G - H_p	[1.6, 2.4]	[-1.5, 0.4]	0.029 ± 0.009	-0.270 ± 0.005	-	-0.023 ± 0.003	-	-	0.01	5.3	270
G - V	[1.6, 2.4]	[-1.5, 0.4]	-0.286 ± 0.104	0.191 ± 0.107	-0.110 ± 0.028	-0.017 ± 0.003	-	-	0.01	3.9	274
G - B_T	[1.6, 2.4]	[-1.4, 0.4]	-0.375 ± 0.257	-0.194 ± 0.267	-0.218 ± 0.069	-0.201 ± 0.009	-	-	0.03	12.7	241
G - V_T	[1.6, 2.4]	[-1.5, 0.4]	-0.261 ± 0.115	0.122 ± 0.119	-0.109 ± 0.031	-0.034 ± 0.006	-0.016 ± 0.007	-	0.01	3.5	272
G - J	[1.6, 3.6]	[-4.8, 1.0]	0.256 ± 0.021	0.510 ± 0.019	0.027 ± 0.004	0.016 ± 0.002	0.005 ± 0.001	-	0.02	0.2	2178
V - J	[1.6, 2.4]	[-1.5, 0.4]	-0.028 ± 0.026	0.880 ± 0.013	-	-	-	-	0.03	2.4	200
V - K_s	[1.6, 2.4]	[-1.5, 0.4]	0.326 ± 0.231	0.786 ± 0.237	0.112 ± 0.061	0.019 ± 0.008	-	-	0.01	2.1	279
J - K_s	[1.6, 3.6]	[-4.8, 1.0]	-0.227 ± 0.024	0.466 ± 0.021	-0.023 ± 0.005	-0.016 ± 0.002	-0.005 ± 0.001	-	0.02	0.1	2180
$B_T - V_T$	[1.6, 2.4]	[-1.5, 0.4]	-0.247 ± 0.023	0.713 ± 0.012	-	0.175 ± 0.007	-	-	0.03	8.0	254
g - r	[1.6, 3.1]	[-2.4, 0.4]	-0.263 ± 0.010	0.521 ± 0.005	-	0.079 ± 0.006	0.015 ± 0.004	-	0.03	8.8	465
g - i	[1.6, 3.1]	[-1.4, 0.4]	0.280 ± 0.084	0.057 ± 0.079	0.163 ± 0.018	0.063 ± 0.005	-	-	0.03	13.5	282
r - i	[1.6, 3.1]	[-1.4, 0.4]	0.236 ± 0.050	-0.171 ± 0.047	0.095 ± 0.011	-	-	-	0.02	2.2	364
G - W1	[1.6, 3.2]	[-2.4, 0.5]	0.099 ± 0.043	0.948 ± 0.040	0.019 ± 0.009	0.006 ± 0.004	0.007 ± 0.003	-	0.03	0.4	1666
W1 - W2	[1.6, 3.2]	[-2.4, 0.5]	0.065 ± 0.039	-0.051 ± 0.038	-0.014 ± 0.009	0.049 ± 0.015	0.007 ± 0.002	-0.028 ± 0.008	0.02	0.1	1657
W2 - W3	[1.6, 3.2]	[-2.4, 0.5]	-0.228 ± 0.032	0.240 ± 0.029	-0.038 ± 0.006	-	-	-	0.03	0.1	1671
H - W2	[1.6, 3.2]	[-2.4, 0.5]	0.025 ± 0.008	0.032 ± 0.004	-	0.009 ± 0.004	0.016 ± 0.003	-	0.03	0.4	1137

Table 2. Coefficients and range of applicability of the \hat{T} vs $G - K_s$ relation (top table) and of the $[\hat{T}, G - K_s]$ relation (bottom table): $Y = a_0 + a_1 X + a_2 X^2 + a_3 [\text{Fe}/\text{H}] + a_4 [\text{Fe}/\text{H}]^2 + a_5 X [\text{Fe}/\text{H}]$. We remind that $\hat{T} = T_{\text{eff}}/5040$. Note that the range of temperatures of the $[\hat{T}, G - K_s]$ calibration (second table) is given in T_{eff} (not \hat{T})

T_{eff}	$G - K_s$ range	[Fe/H] range	a_0	a_1	a_2	a_3	a_4	a_5	RMS $_{[T_{\text{eff}}(K)]}$	%outliers	N
\hat{T}	[1.6, 3.7]	[-2.2, 0.4]	1.648 ± 0.027	-0.455 ± 0.023	0.054 ± 0.005	0.088 ± 0.012	0.001 ± 0.002	-0.026 ± 0.006	59	1.3	523

Colour	T_{eff} range (K)	[Fe/H] range	a_0	a_1	a_2	a_3	a_4	a_5	RMS $_{[G-K_s]}$	%outliers	N
$G - K_s$	[3603.7, 5207.7]	[-2.2, 0.4]	13.554 ± 0.478	-20.429 ± 1.020	8.719 ± 0.545	0.143 ± 0.013	-0.0002 ± 0.009	-	0.05	1.3	523

4.3. Comparison with other studies

In order to test the metallicity-dependent $T_{\text{eff}}C$ calibration derived in the current work, we took advantage of the already existing effective temperature relations provided by some studies. The closest literature relations to our \hat{T} vs $G - K_s$ calibration are T_{eff} vs $V - K_s$. We therefore selected a sample of APOGEE stars, with photometry information on the G , V and K_s bands, and satisfying the quality criteria specified in Section 2. This gave us 179 stars for the test. Their effective temperatures were calculated by using our \hat{T} vs $G - K_s$ relation and through the T_{eff} vs $V - K_s$ relations from three different studies:

- Ramírez & Meléndez (2005): calibrations for main-sequence and giant stars based on temperatures derived with the infrared flux method (IRFM). They are valid within a range of temperatures and metallicities of 4000 K - 7000 K and $-3.5 \leq [\text{Fe}/\text{H}] \leq 0.4$, respectively, and spectral types F0 to K5. The calibrations were done using a sample of more than 100 stars with known UBV , $uvby$, Vilnius, Geneva, RI (Cousins), DDO, Hipparcos-Tycho and 2MASS photometric bands.
- González Hernández & Bonifacio (2009): also with the IRFM, they derived a new effective temperature scale for FGK stars, by using the 2MASS catalogue and theoretical fluxes computed from ATLAS models. Their T_{eff} -colour calibrations obtained with these temperatures are especially meant to be good for metal-poor stars. The calibrations were done using Johnson-Cousins $BV(RI)$, the 2MASS JHK_s photometric bands and the Strömgren $b - y$ colour index

- Huang et al. (2015): calibrations for dwarfs and giants based on a collection from the literature of about two hundred nearby stars (including 54 giants) with direct interferometry effective temperature measurements. Their giant's calibrations are valid for an effective temperature range of 3100 K - 5700 K and spectral types K5 to G5. The calibrations were done using Johnson $UBVR_1JHK$, the Cousins $I_C R_C$, the 2MASS JHK_s and the SDSS gr photometric bands

Fig. 6 shows the residuals of the effective temperatures obtained with these various T_{eff} vs $V - K_s$ literature relations with respect to the T_{eff} derived through our \hat{T} vs $G - K_s$ fit. The differences stay mostly within $\pm 100\text{K}$ (mainly explained by the various sources of effective temperatures together with the different treatment of the interstellar extinction in each case) but with a strong correlation with metallicity. This correlation is stronger than the one documented on the APOGEE DR13 release (see the corresponding discussion in Section 2.6). Applying the suggested correction still leads to a significant correlation with the residuals of the González Hernández & Bonifacio (2009) temperatures, although smaller. For users interested in working in the González Hernández & Bonifacio (2009) [GHB09] temperature scale, we found that, within the range of metallicity tested here, a simple linear relation allows the transformation : $T_{\text{eff}}(\text{GHB09}) = 5040 \hat{T} + 7 - 200 [\text{Fe}/\text{H}]$.

5. The RC absolute magnitudes

To calibrate the absolute magnitudes of the RC, we selected a different sample of stars. Indeed, in order to avoid contamina-

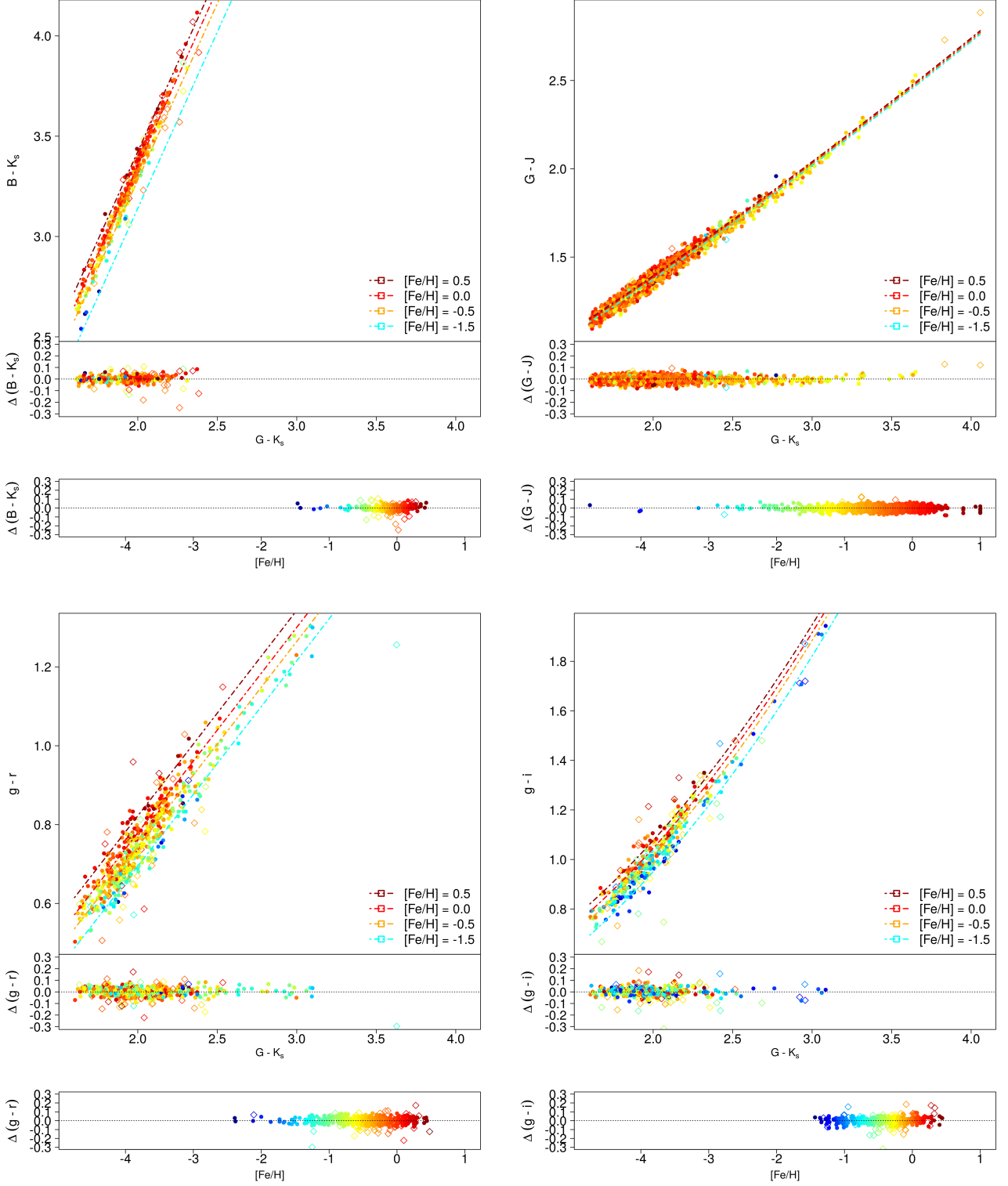


Fig. 4. Empirical colour vs $G - K_s$ calibrations for $B - K_s$, $G - J$, $g - r$ and $g - i$ colour indices. The dash-dotted lines correspond to our calibration at fixed metallicities (see legend). The colour of the points varies as a function of the metallicity. Diamonds correspond to the outliers removed at 3σ during the MCMC process. At the bottom of each calibration plot: residuals of the fit as a function of $G - K_s$ and $[Fe/H]$. All plots are scaled to the same $G - K_s$ colour and metallicity intervals

tion by the Secondary Red Clump (see next Sect. 6), we made use only of stars within $1.93 < G - K_s < 2.3$ and for which M_{K_s} is brighter than -0.5 (similar as in Eq. 2). As in Sect. 2, we kept only low extinction stars (i.e. $E(B - V)_{\max} < 0.01$), with

$\sigma_G < 0.01$ and high photometric quality on the K band. The sample contains 2482 stars. For each band we then applied the same photometric constraints as for the CC and $T_{\text{eff}}C$ calibrations, previously specified in Sect. 2.3.

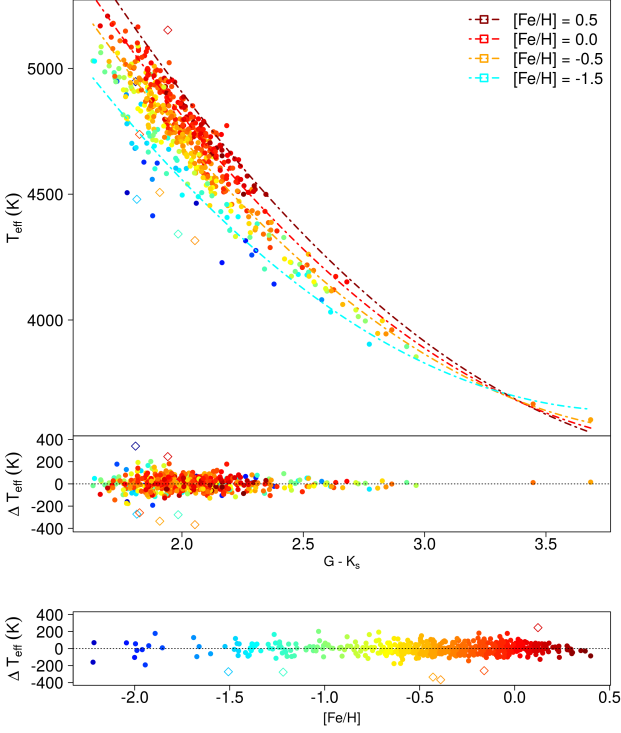


Fig. 5. Empirical normalised effective temperature versus $G - K_s$ calibration. The dash-dotted lines correspond to our calibration at fixed metallicities (see legend). The colour of the points varies as a function of the metallicity. Diamonds correspond to the outliers removed at 3σ during the MCMC process. At the bottom: residuals of the fit as a function of $G - K_s$ and $[\text{Fe}/\text{H}]$

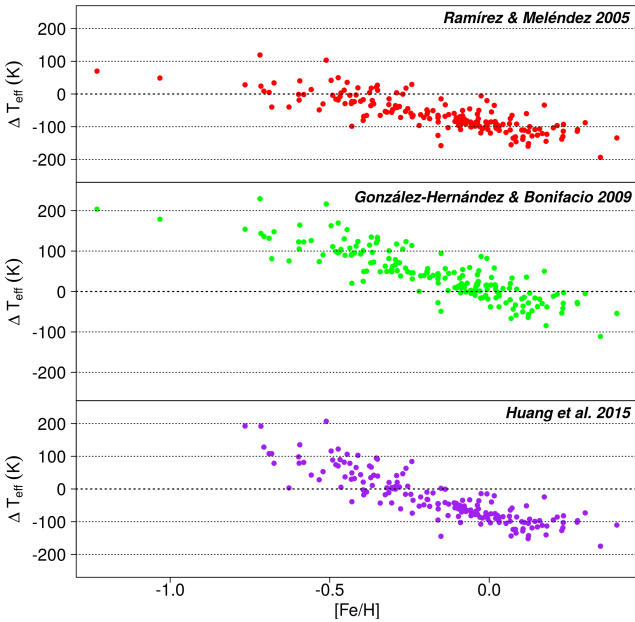


Fig. 6. Residuals of the effective temperatures obtained through the T_{eff} vs $V - K_s$ calibrations of Ramírez & Meléndez (2005) (top panel, red), González Hernández & Bonifacio (2009) (middle panel, green) and Huang et al. (2015) (bottom panel, purple), with respect to the values derived with the \hat{T} vs $G - K_s$ fit of this work, for a sample of 179 APOGEE stars with high photometric quality and low interstellar extinction.

Considering the strong contamination of the RC by the RGB bump and the variation of both the RC and the RGB bump with colour, we did not estimate the RC absolute magnitude through a Gaussian fit to the magnitude distribution but through the mode of the distribution. The mode estimate is also less sensitive to the sample selection function. To model the colour dependency we looked for the maximum of $Q(\alpha, \beta)$, a kernel based distribution function of the residuals $M_\lambda - (\alpha(G - K_s) + \beta)$, with M_λ the absolute magnitude of each particular band.

$$\max_{(\alpha, \beta)} Q(\alpha, \beta) = \sum_{i=1}^N \phi(\alpha + \beta (G - K_s - 2.1) - M_\lambda) \quad (5)$$

where the constant 2.1, the median of $G - K_s$ of the sample, allows to center the fit on the RC.

The kernel ϕ we used corresponds to a Gaussian model of the parallax errors converted in magnitude space (we neglected here the photometric errors):

$$\phi = P_M(M|M_0) = P_\varpi(\varpi(M)|\varpi_0) \frac{\partial \varpi}{\partial M} \quad (6)$$

$$\phi(\alpha + \beta (G - K_s) - M_\lambda) \propto \mathcal{N}(\varpi_{\alpha, \beta, G}, \varpi, \sigma_\varpi) \varpi_{\alpha, \beta, m_\lambda} \quad (7)$$

$$\text{with } \varpi_{\alpha, \beta, m_\lambda} = 10^{(\alpha + \beta (G - K_s) - m_\lambda - 5)/5}$$

This method allows to work directly with the parallaxes without selection in relative precision, avoiding the corresponding biases.

In Table 3 we summarise the results obtained with this method for 15 photometric bands. The initial uncertainties obtained through the maximum optimization algorithm appeared underestimated (~ 0.004). Indeed we saw that by changing slightly the sample selection the results changed by more than the quoted errors. We provide in Table 3 the uncertainties by Bootstrap instead.

We have checked the degree of significance of the colour term for each relationship through a p-value test at 99% confidence level. We find a marginal dependence on colour for M_{K_s} (p-value of 0.004) as well as for M_H (p-value of 0.002), negligible for M_{W1} , M_{W2} , M_{W3} and M_{W4} , and an important dependence for M_G and the other magnitudes. For those magnitudes for which there is no significant dependence we provide the results computed with β fixed to zero (indicated with "-" in the table). We also include in Table 3 the results obtained for M_{K_s} and M_H without taking into account their marginal dependence on colour ($M_{K_s} = -1.606 \pm 0.009$, $M_H = -1.450 \pm 0.017$).

We checked the robustness of the mode estimate versus the selected sample. We found differences of 0.006 mag when selecting only stars with $\sigma_\varpi/\varpi < 10\%$ (1085 stars).

We determined similarly the mode of the RC M_{K_s} distribution according to the Padova isochrones, simulating an HR diagram with a constant Star Formation Rate (SFR), a Chabrier (2001) Initial Mass Function (IMF), and a Gaussian metallicity distribution (0, 0.02). We obtained $M_{K_s} = -1.660 \pm 0.003$, in agreement with Bovy et al. (2014). We checked on this simulation that indeed the mode is robust to changes in the SFR, the IMF and the Age-Metallicity Ratio (AMR) hypothesis.

A summary of various absolute magnitude calibrations in the literature can be found in Table 4, based on Table 1 of Girardi (2016) and complemented with more recent studies. In this table we indicate, for comparison purposes, our result from Table

Table 3. Coefficients of the absolute magnitude calibrations of the RC: $M_\lambda = \alpha + \beta (G - K_s - 2.1)$

M_λ	α	β	N
M_B	1.931 ± 0.009	2.145 ± 0.130	1043
M_V	0.855 ± 0.009	1.354 ± 0.126	1113
M_{B_T}	2.239 ± 0.009	2.397 ± 0.135	1190
M_{V_T}	0.975 ± 0.009	1.447 ± 0.127	1639
M_g	1.331 ± 0.056	1.961 ± 0.585	407
M_r	0.552 ± 0.026	1.194 ± 0.289	340
M_i	0.262 ± 0.032	0.626 ± 0.402	243
M_G	0.495 ± 0.009	1.121 ± 0.128	2482
M_J	-0.945 ± 0.010	0.421 ± 0.117	2098
M_H	-1.454 ± 0.018	0.234 ± 0.224	1315
M_H^*	-1.450 ± 0.017	-	1315
M_{K_s}	-1.605 ± 0.009	0.121 ± 0.125	2482
$M_{K_s}^*$	-1.606 ± 0.009	-	2482
M_{W1}	-1.711 ± 0.017	-	962
M_{W2}	-1.585 ± 0.016	-	1031
M_{W3}	-1.638 ± 0.011	-	2026
M_{W4}	-1.704 ± 0.012	-	747

Notes. (*) Result without taking into account the marginal dependence on colour (p-value < 0.005)

3 assuming $G - K_s$ colour equal to 2.1 when the external calibrations did not consider a colour effect while we found such a dependency.

We found general agreement with the M_{K_s} from previous works who mainly used Hipparcos data. The M_{K_s} value of Alves (2000) is in the TMSS system (Bessell & Brett 1988), while the others, including this work, mainly used 2MASS data. However the quality flags considered to select the data are not the same in each case. Our M_{K_s} value of the mean RC K-band absolute magnitude appears to be slightly lower than in Alves (2000), Grocholski & Sarajedini (2002) and Laney et al. (2012), but higher than the values in van Helshoecht & Groenewegen (2007), Groenewegen (2008) and Francis & Anderson (2014). It perfectly agrees with the last result of Hawkins et al. (2017) using also Gaia data but with a very different selection function and handling of the extinction. As in this work, Groenewegen (2008) also found a weak dependency of M_{K_s} on colour.

For M_J , Laney et al. (2012) found a slightly larger result with respect to us. However, the source of photometric data is different from ours, and we have a much larger sample. Chen et al. (2017) used a much smaller sample and their value is even higher than the one from Laney et al. (2012) but still consistent with this work. We find perfect agreement with Hawkins et al. (2017) who also used a sample of Gaia stars. The same authors also calibrated M_H , the results of which are in fair agreement with our value.

Chen et al. (2017) also calibrated the APASS-SLOAN *gri* absolute magnitudes using seismically determined RC stars from the Strömgren survey for Asteroseismology and Galactic Archaeology (SAGA). We find that the RC is less bright in all three magnitudes although within the errors bars.

As shown in Table 4, for M_{W1} our result agrees with both Chen et al. (2017) and Hawkins et al. (2017), and it is marginally brighter than the one from Yaz Gökçe et al. (2013). For M_{W2} we also find good agreement with Chen et al. (2017), however the differences are larger with respect to Hawkins et al. (2017) as they already point out in their article. We have indeed found important variations depending on the sample selection criteria.

In particular, by considering only the high photometric quality flag (i.e. qph = A) and no cut in the observed magnitude, we obtained $M_{W2} = -1.68 \pm 0.01$ with a strong correlation with colour. By removing the saturated stars (Cotten & Song 2016), as described in Section 2.3, this dependence with colour becomes negligible, as it is for the other WISE bands, and the peak is much fainter. This may explain the too bright value found by Hawkins et al. (2017).

With M_{W3} all the works are consistent among them, with the exception of Chen et al. (2017) who obtained a brighter value. And for M_{W4} our result is fainter than the one found for the first time by Hawkins et al. (2017).

Finally, Hawkins et al. (2017) also provided the first calibration of M_G , based on a hierarchical probabilistic model. In this work we provide a different approach by directly using the mode of the distribution, and with a larger sample of data. Their G absolute magnitude is somewhat brighter. As mentioned above, with our method we also find a strong dependence on colour. This may explain the difference between both estimations, together with the fact that they corrected the reddening by deriving the extinction coefficients through the nominal Gaia G band. The updated extinction coefficients will be found in Danielski et al. (2017), in prep.

Besides the parallax accuracy and the various sources of photometric information, one of the main differences between these estimates is the handling of the interstellar extinction: Alves (2000), Stanek & Garnavich (1998), Girardi et al. (1998) and Laney et al. (2012) assumed no reddening, while the other authors corrected their magnitudes using and combining different interstellar laws and/or maps. It is clear that our sample selection based on low extinction stars introduces as well a bias in all our calibrations, although minimally. Indeed, the reddening cut at $E(B - V)_{\max} < 0.01$ corresponds to a maximum overestimation of the absolute magnitude of about 0.02 mag in the G band, while about 0.003 mag in the K band (see Danielski et al. 2017, in prep.).

The discrepancies among the other estimates may also be justified by the different methods used: most of the authors considered a Gaussian fit, while here we used the mode of the distribution.

6. The TGAS RC HRD

Figure 7 shows the TGAS HR diagram for red giant stars for absolute magnitudes in the G and K photometric bands. We used stars listed in Table A.1 (see Appendix A), with low extinction ($E(B - V)_{\max} < 0.015$), 10% parallax precision, $\sigma_G < 0.01$ and 2MASS JK high photometric quality. In both cases the RC is easily detected. However other features may also be observed. Indeed, on the bluest part of the RC we can see a small overdensity belonging to the Secondary Red Clump (Girardi et al. 1998; Girardi 1999), a group of still metal-rich but younger (i.e. slightly more massive) stars that extend the RC to fainter magnitudes (up to 0.4 mag fainter). On the red side of the clump and below it, we find the Red Giant Branch Bump (RGB bump or RGBB), another overdensity of slightly more massive stars than the RC which causes a peak (*bump*) in the luminosity function (see Christensen-Dalsgaard (2015) for a review on this CMD feature).

On the same diagrams we also overplotted the absolute magnitude calibrations obtained in previous Sect. 5 (Table 3).

In Fig. 8 we show again the RC HR diagram but now overplotting in different colours the Padova isochrones (Bressan et al.

Table 4. Comparison of the M_A of this work with other determinations in the literature

M_A	Reference	Calibration	Sample	Extinction correction
M_G	Hawkins et al. (2017)	0.44 ± 0.01	972 TGAS (Gaia DR1)	$E(B - V)$ from 3D dustmap of Green et al. (2015)
	This work	$0.495 \pm 0.009^*$	2482 TGAS (Gaia DR1)	None: low extinction stars selection according to Capitanio et al. (2017) 3D map
M_J	Laney et al. (2012)	-0.984 ± 0.014	191 Revised Hipparcos parallaxes with SAAO JK mag, data corrected for Lutz-Kelker bias	None
	Chen et al. (2017)	-1.016 ± 0.063	$\lesssim 171$ RC stars of the SAGA survey with 2MASS J mag	SAGA $E(B - V)$ with Cardelli et al. (1989) law
	Hawkins et al. (2017)	-0.93 ± 0.01	972 TGAS (Gaia DR1) with 2MASS J mag	E_{B-V} from 3D dustmap of Green et al. (2015)
	This work	$-0.945 \pm 0.01^*$	2098 TGAS (Gaia DR1) with 2MASS J mag	None: low extinction stars selection according to Capitanio et al. (2017) 3D map
M_H	Laney et al. (2012)	-1.490 ± 0.015	191 Revised Hipparcos parallaxes with SAAO JK mag, data corrected for Lutz-Kelker bias	None
	Chen et al. (2017)	-1.528 ± 0.055	$\lesssim 171$ RC stars of the SAGA survey with 2MASS J mag	SAGA $E(B - V)$ with Cardelli et al. (1989) law
	Hawkins et al. (2017)	-1.46 ± 0.01	972 TGAS (Gaia DR1) with 2MASS J mag	E_{B-V} from 3D dustmap of Green et al. (2015)
	This work	-1.450 ± 0.017	1315 TGAS (Gaia DR1) with 2MASS J mag	None: low extinction stars selection according to Capitanio et al. (2017) 3D map
M_K	Alves (2000)	-1.61 ± 0.03	238 Hipparcos RC giants with TMSS K mag	None
	Grocholski & Sarajedini (2002)	-1.61 ± 0.04	14 WYIN Open Clusters	Twarog et al. (1997) $E(B - V)$ with Cardelli et al. (1989) law
	van Helshoecht & Groenewegen (2007)	-1.57 ± 0.05	24 2MASS Open Clusters	Twarog et al. (1997) $E(B - V)$ data
	Groenewegen (2008)	-1.54 ± 0.04	Revised Hipparcos parallaxes with 2MASS K mag	Based on three 3D models
	Laney et al. (2012)	-1.613 ± 0.015	191 Revised Hipparcos parallaxes with SAAO K mag, data corrected for Lutz-Kelker bias	None
	Francis & Anderson (2014)	-1.53 ± 0.01	Revised Hipparcos parallaxes with 2MASS K mag	Outside 100pc: Burstein & Heiles (1978, 1982) map and Bahcall & Soneira (1980) formulae
	Chen et al. (2017)	-1.626 ± 0.057	$\lesssim 171$ RC stars of the SAGA survey with 2MASS K band	SAGA $E(B - V)$ with Cardelli et al. (1989) law
	Hawkins et al. (2017)	-1.61 ± 0.01	972 TGAS (Gaia DR1) with 2MASS K mag	$E(B - V)$ from 3D dustmap of Green et al. (2015)
	This work	-1.606 ± 0.009	2482 TGAS (Gaia DR1) with 2MASS K mag	None: low extinction stars selection according to Capitanio et al. (2017) 3D map
M_g	Chen et al. (2017)	1.229 ± 0.172	$\lesssim 171$ RC stars of the SAGA survey with APASS-SLOAN g mag	SAGA $E(B - V)$ with Cardelli et al. (1989) law
	This work	$1.331 \pm 0.056^*$	407 TGAS (Gaia DR1) with APASS-SLOAN g mag	None: low extinction stars selection according to Capitanio et al. (2017) 3D map
M_r	Chen et al. (2017)	0.420 ± 0.110	$\lesssim 171$ RC stars of the SAGA survey with APASS-SLOAN r mag	SAGA $E(B - V)$ with Cardelli et al. (1989) law
	This work	$0.552 \pm 0.026^*$	340 TGAS (Gaia DR1) with APASS-SLOAN r mag	None: low extinction stars selection according to Capitanio et al. (2017) 3D map
M_i	Chen et al. (2017)	0.157 ± 0.094	$\lesssim 171$ RC stars of the SAGA survey with APASS-SLOAN i mag	SAGA $E(B - V)$ with Cardelli et al. (1989) law
	This work	$0.262 \pm 0.032^*$	243 TGAS (Gaia DR1) with APASS-SLOAN i mag	None: low extinction stars selection according to Capitanio et al. (2017) 3D map
M_{W1}	Yaz Gökçe et al. (2013)	-1.635 ± 0.026	3889 Revised Hipparcos RC parallaxes with WISE $W1$ mag	$E(B - V)$ from 2D map of Schlegel et al. (1998)
	Chen et al. (2017)	-1.694 ± 0.061	$\lesssim 171$ RC stars of the SAGA survey with WISE $W1$ mag	SAGA $E(B - V)$ with Cardelli et al. (1989) law
	Hawkins et al. (2017)	-1.68 ± 0.02	936 TGAS (Gaia DR1) with WISE $W1$ mag	$E(B - V)$ from 3D dustmap of Green et al. (2015)
	This work	-1.711 ± 0.017	962 TGAS (Gaia DR1) with WISE $W1$ mag	None: low extinction stars selection according to Capitanio et al. (2017) 3D map
M_{W2}	Chen et al. (2017)	-1.595 ± 0.064	$\lesssim 171$ RC stars of the SAGA survey with WISE $W2$ mag	SAGA $E(B - V)$ with Cardelli et al. (1989) law
	Hawkins et al. (2017)	-1.69 ± 0.02	934 TGAS (Gaia DR1) with WISE $W2$ mag	$E(B - V)$ from 3D dustmap of Green et al. (2015)
	This work	-1.585 ± 0.016	1031 TGAS (Gaia DR1) with WISE $W2$ mag	None: low extinction stars selection according to Capitanio et al. (2017) 3D map
M_{W3}	Yaz Gökçe et al. (2013)	-1.606 ± 0.024	3889 Revised Hipparcos RC parallaxes with WISE $W3$ mag	$E(B - V)$ from 2D map of Schlegel et al. (1998)
	Chen et al. (2017)	-1.752 ± 0.068	$\lesssim 171$ RC stars of the SAGA survey with WISE $W3$ mag	SAGA $E(B - V)$ with Cardelli et al. (1989) law
	Hawkins et al. (2017)	-1.67 ± 0.02	936 TGAS (Gaia DR1) with WISE $W3$ mag	$E(B - V)$ from 3D dustmap of Green et al. (2015)
	This work	-1.638 ± 0.011	2026 TGAS (Gaia DR1) with WISE $W3$ mag	None: low extinction stars selection according to Capitanio et al. (2017) 3D map
M_{W4}	Hawkins et al. (2017)	-1.76 ± 0.01	910 TGAS (Gaia DR1) with WISE $W4$ mag	$E(B - V)$ from 3D dustmap of Green et al. (2015)
	This work	-1.704 ± 0.012	747 TGAS (Gaia DR1) with WISE $W4$ mag	None: low extinction stars selection according to Capitanio et al. (2017) 3D map

Notes. ^(*) Result from Table 3 assuming $G - K_s$ colour equal to 2.1

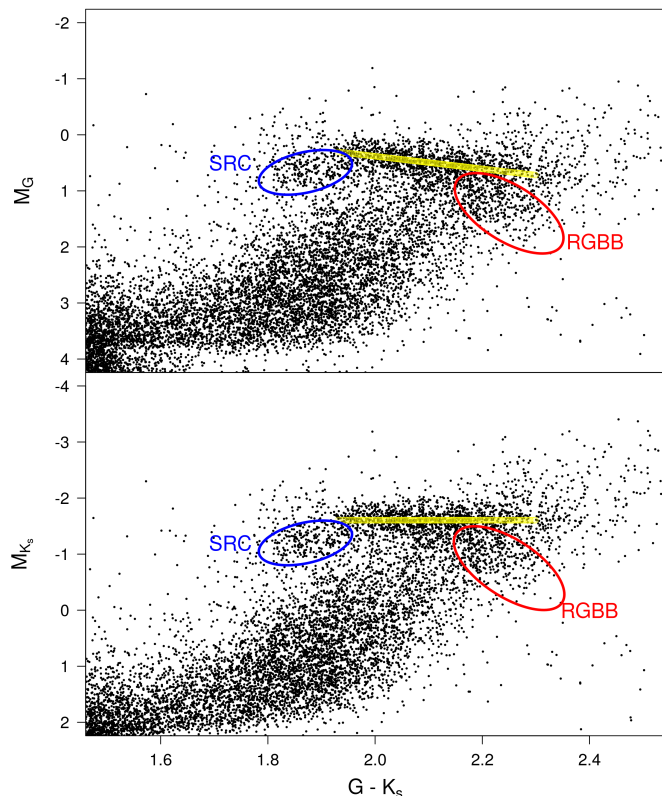


Fig. 7. TGAS HR diagram of the RC region for the M_G (top) and the M_{K_s} (bottom) absolute magnitudes, using stars with $E(B - V)_{\max} < 0.015$, 10% parallax precision, $\sigma_G < 0.01$ and 2MASS JK high photometric quality. The location of the Secondary Red Clump (SRC) and the Red Giant Branch Bump (RGBB) features are easily observed on the diagram. We have highlighted them in blue and red, respectively. The yellow line shows the absolute magnitude calibration obtained in this work

2012, Parsec 2.7) at different metallicities (top panel) and at different ages (bottom panel). We use the original T_{eff} from the isochrones and applied our $G - K_s$ vs \hat{T} calibration (Table 2) to derive the colour $G - K_s$.

We may see that while the position of the RC seems to nicely fit the isochrones, the RGB bump is slightly too bright in the isochrones. Following the process in Sect. 5, we found a difference of -0.07 mag between the Padova RC and the TGAS RC, and about 0.2 mag for the RGB bump.

7. Conclusions

Using the First Gaia Data Release parallaxes and photometry, the new 3D interstellar extinction map of Capitanio et al. (2017), the 2MASS catalogue and the last APOGEE release (DR13), a complete photometric calibration including colours (spread from visual to infrared wavelengths), absolute magnitudes, spectroscopic metallicities, and homogeneous effective temperatures, is provided in this work for solar neighbourhood RC stars. We have made use of high photometric quality data from the Gaia, Johnson, 2MASS, Hipparcos, Tycho-2 and APASS-SLOAN and WISE photometric systems.

A robust MCMC method accounting for all variable uncertainties was developed to derive 20 accurate metallicity-dependent colour-colour relations and the \hat{T} vs $G - K_s$ and

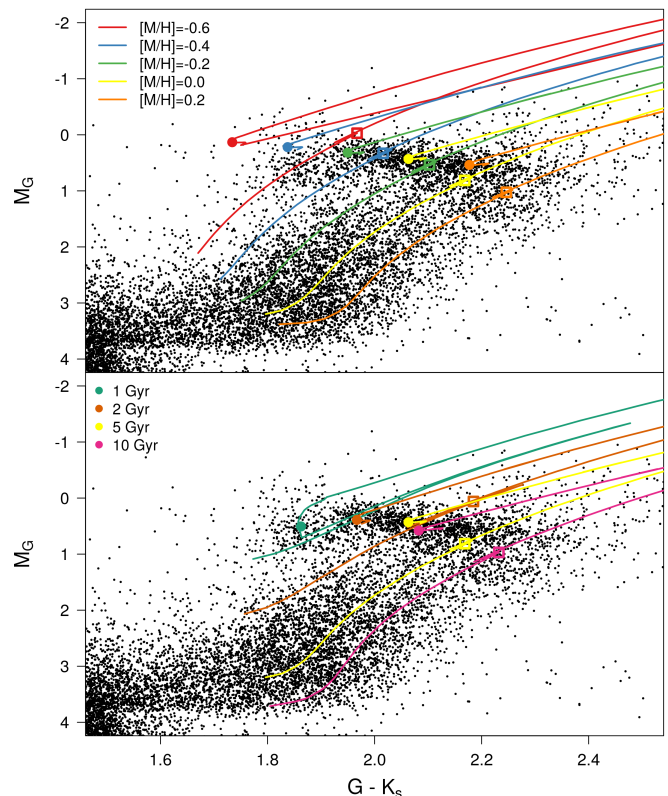


Fig. 8. Padova isochrones overlaid on the Gaia DR1 HRD. Top: isochrones for an age of 5 Gyr and different metallicities. Bottom: isochrones for a solar metallicity and different ages. Circles correspond to the Red Clump location, squares to the RGB bump

$G - K_s$ vs \hat{T} fits (with \hat{T} the normalized effective temperature, $\hat{T} = T_{\text{eff}}/5040$). We checked that the effective temperature calibration is compatible with those from Ramírez & Meléndez (2005), González Hernández & Bonifacio (2009) and Huang et al. (2015) within the metallicity and colour ranges of applicability.

We also derived the absolute magnitudes for the TGAS RC on 15 photometric bands (including M_G and M_{K_s}) through a kernel based magnitude distribution method, and using the largest high quality dataset used so far for an absolute magnitude calibration of the RC. We obtained a small dependence on colour for M_{K_s} and M_H , not-significant for M_{W1} , M_{W2} , M_{W3} and M_{W4} , but important for M_G and the other magnitudes.

Note that all these photometric relationships will be improved in later Gaia releases as well as extended to other photometric bands, when larger Red Clump samples will be available.

We presented an un-reddened TGAS HR diagram for the RC region, in which we can already easily identify other features of red giant stars, such as the Secondary Red Clump and the Red Giant Branch Bump. By using our calibrations we could compare the Padova isochrones with the TGAS HR diagram and found good agreement with the RC location on the diagram, although the RGB bump appears too bright in the isochrones.

The photometric calibrations presented here are being used to derive k_G , the interstellar extinction coefficient in the G -band (Danielski et al. 2017, in prep.), and to provide photometric interstellar extinctions of large surveys like APOGEE to be in-

cluded in the next release of the new 3D extinction map of Capitanio et al. (2017).

In summary, this work used the high quality of the Gaia DR1 data to calibrate the Gaia Red Clump. In turn, these calibrations can be used as the second rung of the cosmic distance ladder. Indeed, together with asteroseismic constraints, we can now derive the distance modulus of a large sample of RC stars. By choosing RC stars distant enough so that their estimated distance uncertainty is better than the Gaia parallax precision, these stars may be used to check the zero point of the Gaia parallaxes and their precision (Arenou et al. 2017). This is already being applied within the Gaia Data Release 2 verification process.

Acknowledgements. L.R.-D. acknowledges financial support from the *Centre National d'Etudes Spatiales* (CNES) fellowship program. This work has made use of data from the European Space Agency (ESA) mission *Gaia* (<https://www.cosmos.esa.int/gaia>), processed by the *Gaia* Data Processing and Analysis Consortium (DPAC, <https://www.cosmos.esa.int/web/gaia/dpac/consortium>). Funding for the DPAC has been provided by national institutions, in particular the institutions participating in the *Gaia* Multilateral Agreement. This publication makes use of data products from the Two Micron All Sky Survey, which is a joint project of the University of Massachusetts and the Infrared Processing and Analysis Center/California Institute of Technology, funded by the National Aeronautics and Space Administration and the National Science Foundation. L.R.-D. acknowledges support from *Agence Nationale de la Recherche* through the STILISM project (ANR-12-BS05-0016-02). This research has also made use of VizieR databases operated at the *Centre de Données astronomiques de Strasbourg* (CDS) in France.

References

- Adibekyan, V. Z., Sousa, S. G., Santos, N. C., et al. 2012, *A&A*, 545, A32
- Alves, D. R. 2000, *ApJ*, 539, 732
- Alves, S., Benamati, L., Santos, N. C., et al. 2015, *MNRAS*, 448, 2749
- Arenou, F., Luri, X., Babusiaux, C., et al. 2017, *A&A*, 599, A50
- Aringer, B., Girardi, L., Nowotny, W., Marigo, P., & Bressan, A. 2016, *MNRAS*, 457, 3611
- Bahcall, J. N. & Soneira, R. M. 1980, *ApJS*, 44, 73
- Bensby, T., Feltzing, S., & Oey, M. S. 2014, *A&A*, 562, A71
- Bessell, M. S. & Brett, J. M. 1988, *PASP*, 100, 1134
- Bovy, J., Nidever, D. L., Rix, H.-W., et al. 2014, *AJ*, 790, 127
- Bressan, A., Marigo, P., Girardi, L., et al. 2012, *MNRAS*, 427, 127
- Bruntt, H., Basu, S., Smalley, B., et al. 2012, *MNRAS*, 423, 122
- Burstein, D. & Heiles, C. 1978, *Astrophys. Lett.*, 19, 69
- Burstein, D. & Heiles, C. 1982, *AJ*, 87, 1165
- Capitanio, L., Lallement, R., Vergely, J. L., Elyajouri, M., & Monreal-Ibero, A. 2017, *ArXiv e-prints* [[arXiv:1706.07711](https://arxiv.org/abs/1706.07711)]
- Cardelli, J. A., Clayton, G. C., & Mathis, J. S. 1989, *AJ*, 345, 245
- Chabrier, G. 2001, *ApJ*, 554, 1274
- Chen, Y. Q., Casagrande, L., Zhao, G., et al. 2017, *ArXiv e-prints* [[arXiv:1704.03903](https://arxiv.org/abs/1704.03903)]
- Christensen-Dalsgaard, J. 2015, *MNRAS*, 453, 666
- Cotten, T. H. & Song, I. 2016, *ApJS*, 225, 15
- Cutri, R. M., Skrutskie, M. F., van Dyk, S., et al. 2003, *VizieR Online Data Catalog*, 2246
- da Silva, R., Milone, A. d. C., & Rocha-Pinto, H. J. 2015, *A&A*, 580, A24
- Danielski, C., Babusiaux, C., Ruiz-Dern, L., Sartoretti, P., & Lallement, R. 2017, in prep.
- De Pascale, M., Worley, C. C., de Laverny, P., et al. 2014, *A&A*, 570, A68
- Evans, D. W., Riello, M., De Angeli, F., et al. 2017, *ArXiv e-prints* [[arXiv:1701.05873](https://arxiv.org/abs/1701.05873)]
- Fabrigius, C., Høg, E., Makarov, V. V., et al. 2002, *A&A*, 384, 180
- Francis, C. & Anderson, E. 2014, *MNRAS*, 441, 1105
- Gaia Collaboration, Brown, A. G. A., Vallenari, A., et al. 2016a, *A&A*, 595, A2
- Gaia Collaboration, Brown, A. G. A., Vallenari, A., et al. 2016b, *A&A*, 595, A2
- García Pérez, A. E., Allende Prieto, C., Holtzman, J. A., et al. 2016, *AJ*, 151, 144
- Girardi, L. 1999, *ArXiv Astrophysics e-prints* [[astro-ph/9912309](https://arxiv.org/abs/astro-ph/9912309)]
- Girardi, L. 2016, *ARA&A*, 54, 95
- Girardi, L., Groenewegen, M. A. T., Weiss, A., & Salaris, M. 1998, *MNRAS*, 301, 149
- González Hernández, J. I. & Bonifacio, P. 2009, *A&A*, 497, 497
- Green, G. M., Schlafly, E. F., Finkbeiner, D. P., et al. 2015, *ApJ*, 810, 25
- Grocholski, A. J. & Sarajedini, A. 2002, *AJ*, 123, 1603
- Groenewegen, M. A. T. 2008, *A&A*, 488, 935
- Hawkins, K., Leistedt, B., Bovy, J., & Hogg, D. W. 2017, *ArXiv e-prints* [[arXiv:1705.08988](https://arxiv.org/abs/1705.08988)]
- Henden, A. A., Templeton, M., Terrell, D., et al. 2016, *VizieR Online Data Catalog*, 2336
- Høg, E., Fabricius, C., Makarov, V. V., et al. 2000, *A&A*, 355, L27
- Holtzman, J. A., Shetrone, M., Johnson, J. A., et al. 2015, *AJ*, 150, 148
- Huang, Y., Liu, X.-W., Yuan, H.-B., et al. 2015, *MNRAS*, 454, 2863
- Jofré, E., Petrucci, R., Saffe, C., et al. 2015, *A&A*, 574, A50
- Jordi, C., Gebran, M., Carrasco, J. M., et al. 2010, *A&A*, 523, A48
- Kovtyukh, V. V., Soubiran, C., Bienaymé, O., Mishenina, T. V., & Belik, S. I. 2006, *MNRAS*, 371, 879
- Kunder, A., Kordopatis, G., Steinmetz, M., et al. 2017, *AJ*, 153, 75
- Lallement, R., Vergely, J.-L., Valette, B., et al. 2014, *A&A*, 561, A91
- Laney, C. D., Jone, M. D., & Pietrzynski, G. 2012, *VizieR Online Data Catalog*, 741
- Lindgren, L., Lammers, U., Bastian, U., et al. 2016, *A&A*, 595, A4
- Luck, R. E. 2015, *AJ*, 150, 88
- Luo, A.-L., Zhao, Y.-H., Zhao, G., et al. 2016, *VizieR Online Data Catalog*, 5149
- Maldonado, J. & Villaver, E. 2016, *A&A*, 588, A98
- Martell, S. L., Sharma, S., Buder, S., et al. 2017, *MNRAS*, 465, 3203
- Morel, T., Miglio, A., Lagarde, N., et al. 2014, *A&A*, 564, A119
- Mortier, A., Santos, N. C., Sousa, S. G., et al. 2013, *A&A*, 558, A106
- Paczynski, B. & Stanek, K. Z. 1998, *ApJ*, 494, L219
- Perryman, M., Agency, E. S., & Consortium, F. 1997, *The Hipparcos and Tycho Catalogues: The Hipparcos catalogue*, ESA SP (ESA Publications Division)
- Plummer, M. 2008, *Biostatistics*, 9, 523
- Pourbaix, D., Tokovinin, A. A., Batten, A. H., et al. 2009, *VizieR Online Data Catalog*, 1
- Pourbaix, D., Tokovinin, A. A., Batten, A. H., et al. 2004, *A&A*, 424, 727
- Puzeras, E., Tautvaisiene, G., Cohen, J. G., et al. 2010, *MNRAS*, 408, 1225
- Ramírez, I., Bajkova, A. T., Bobylev, V. V., et al. 2014a, *ApJ*, 787, 154
- Ramírez, I. & Meléndez, J. 2005, *ApJ*, 626, 446
- Ramírez, I., Meléndez, J., & Asplund, M. 2013, *VizieR Online Data Catalog*, 356
- Ramírez, I., Meléndez, J., Bean, J., et al. 2014b, *A&A*, 572, A48
- Saguner, T., Munari, U., Fiorucci, M., & Vallenari, A. 2011, *A&A*, 527, A40
- Schlafly, E. F. & Finkbeiner, D. P. 2011, *ApJ*, 737, 103
- Schlegel, D. J., Finkbeiner, D. P., & Davis, M. 1998, *ApJ*, 500, 525
- SDSS Collaboration, Albareti, F. D., Allende Prieto, C., et al. 2016, *ArXiv e-prints* [[arXiv:1608.02013](https://arxiv.org/abs/1608.02013)]
- Soubiran, C., Le Campion, J.-F., Brouillet, N., & Chemin, L. 2016, *A&A*, 591, A118
- Stanek, K. Z. & Garnavich, P. M. 1998, *ApJ*, 503, L131
- Takeda, Y., Sato, B., & Murata, D. 2008, *PASJ*, 60, 781
- Thygesen, A. O., Frandsen, S., Bruntt, H., et al. 2012, *A&A*, 543, A160
- Twarog, B. A., Ashman, K. M., & Anthony-Twarog, B. J. 1997, *AJ*, 114, 2556
- Udalski, A. 2000, *ApJ*, 531, L25
- Valentini, M. & Munari, U. 2010, *A&A*, 522, A79
- van Helshoecht, V. & Groenewegen, M. A. T. 2007, *A&A*, 463, 559
- van Leeuwen, F., Evans, D. W., De Angeli, F., et al. 2017, *A&A*, 599, A32
- Wright, E. L., Eisenhardt, P. R. M., Mainzer, A. K., et al. 2010, *AJ*, 140, 1868
- Yaz Gökçe, E., Bilir, S., Öztürkmen, N. D., et al. 2013, *New A*, 25, 19
- Zieliński, P., Niedzielski, A., Wolszczan, A., Adamów, M., & Nowak, G. 2012, *A&A*, 547, A91

Appendix A: Low extinction TGAS HR Catalogue at CDS

Table A.1 contains a few rows of the low extinction TGAS HRD compilation used in this work. The full table is available in VizieR.

The catalogue includes 142996 stars with:

- Gaia DR1 and 2MASS identifiers
- Gaia DR1 parallaxes with precision better than 10%
- Gaia DR1 G magnitude with uncertainties lower than 0.01 mag
- 2MASS J and K_s photometric bands with high quality (i.e. flag q2M = "A.A") and uncertainties lower than 0.03 mag
- Reddening $E(B - V)_{\max} < 0.015$ according to the Capitanio et al. (2017) 3D interstellar extinction map, and the Schlegel et al. (1998) 2D map for stars for which the distance go beyond the 3D map borders

Table A.1. First rows of the low extinction and high photometric and astrometric quality TGAS HRD catalogue

GDR1 id	2MASS id	ϖ	σ_{ϖ}	G	σ_G	J_s	σ_{J_s}	K_s	σ_{K_s}	$E(B - V)_{\max}$
7627862074752	03000819+0014074	6.353	0.308	7.991	0.001	6.606	0.023	6.019	0.020	0.011
16527034310784	03003397+0021355	8.663	0.256	9.972	0.001	8.993	0.018	8.651	0.025	0.004
26834955821312	03000244+0021039	6.202	0.247	9.971	0.001	9.189	0.023	8.860	0.025	0.012
44358422235136	03020031+0029521	9.958	0.548	9.317	0.004	8.332	0.023	7.990	0.024	0.003
115723598973952	03002534+0048455	10.550	0.232	10.788	0.000	9.502	0.022	8.921	0.020	0.003
122732985598464	03004702+0059362	6.582	0.303	8.774	0.001	8.071	0.026	7.833	0.020	0.010
308619170261760	02572363+0058185	7.446	0.279	10.465	0.001	9.437	0.026	8.969	0.023	0.006
310337157179392	02572548+0059538	7.381	0.247	10.592	0.001	9.513	0.023	9.102	0.021	0.007
320713798164992	02585888+0104389	7.481	0.284	9.993	0.002	9.094	0.026	8.728	0.020	0.007
349369819955456	02580800+0122163	6.770	0.261	9.469	0.001	8.573	0.026	8.255	0.027	0.009
...